Resource Management and Cell Planning in LTE Systems

Giovanni Giambene, Tara Ali Yahiya, van Anh Le, Krzysztof Grochla, Konrad Polys

Resource Management and Cell Planning in LTE Systems

Giovanni Giambene[1](✉), Tara Ali Yahiya[2], Van Anh Le[1], Krzysztof Grochla[3], and Konrad Połys[3]

[1] University of Siena, Via Roma, 56, 53100 Siena, Italy
giambene@unisi.it
[2] Laboratoire de Recherche En Informatique, University of Paris-Sud, Orsay, France
[3] Institute of Theoretical and Applied Informatics of PAS, Baltycka 5, 44-100 Gliwice, Poland

Abstract. Future 4G cellular systems will address the need for capacity increase for the support of diverse services. It is therefore of fundamental importance to design innovative 4G cellular systems able to support the increase in the traffic demand. This Chapter deals with LTE systems and the design of a new reuse scheme, called *Soft Frequency Reuse* (SFR), that is able to increase the cell capacity that is studied, considering the impact of different scheduling schemes and of different user mobility patterns. A consistent SFR scenario has been implemented in both Ns-3 and OMNeT++ environments. An analytical approach is proposed to evaluate the cell capacity with SFR that has been validated by means of Ns-3 simulations. Finally, OMNeT++ simulations have permitted to highlight the significant impact of the scheduling scheme and user mobility on cell capacity; different mobility patterns have been taken into account.

Keywords: LTE · Cell planning · Soft frequency reuse

1 Introduction

Digital information and data traffic are experiencing an exponential worldwide growth that represents a challenge to be addressed by network planners [1]. In this scenario, mobile communications will play a major role because broadband wireless connections have surpassed wired ones since 2011. This is the scenario that future 5G systems will have to deal with. *Long Term Evolution* (LTE) is popularly known as a 4G technology and can be considered as the technology of choice for most existing *Third Generation Partnership Project* (3GPP) and 3GPP2 mobile operators, since it will provide economy of scale and an efficient use of the radio spectrum [2]. LTE, whose radio access is called *Evolved UMTS Terrestrial Radio Access Network* (E-UTRAN), is expected to substantially improve end-user throughput, cell capacity and reduce user plane latency, bringing significantly-improved user experience with full mobility support. With the emergence of the *Internet Protocol* (IP) as the protocol of choice

for carrying all traffic types, LTE is expected to provide support for IP-based traffic with end-to-end *Quality of Service* (QoS) [3].

In the LTE architecture, E-UTRAN consists of a single node, i.e., the *eNode B* (eNB) that interfaces with the *User Equipment* (UE). The protocol architecture of the LTE air interface can be separated between control and user planes. In the user plane, the application creates data packets that are processed by protocols such as TCP, UDP and IP; instead, in the control plane, the *Radio Resource Control* (RRC) protocol generates the signalling messages (radio resource management, admission control, enforcement of QoS negotiated, ciphering/deciphering of user and control plane data, compression/decompression of downlink/uplink user plane packet headers, etc.) that are exchanged between eNB and UE. In both cases, the information is processed by the *Packet Data Convergence Protocol* (PDCP), the *Radio Link Control* (RLC) protocol, and the *Medium Access Control* (MAC) protocol, before being passed to the physical layer (PHY) for transmissions. IP packet segmentation is performed at the RLC layer.

The aim of this Chapter is to analyse a special frequency reuse scheme proposed for LTE and called *Soft Frequency Reuse* (SFR). The interest is to study SFR with both analysis and simulations in order to determine the configuration that permits us to maximize cell capacity. This work represents a significant improvement with respect to the study carried out in [3], where we have adopted a less accurate modelling of SFR and where we have not conducted a simulation study to validate the analysis proposed. We expect that the present work can help network planners when designing 4G LTE systems based on SFR.

1.1 LTE Key Features and Radio Resources

LTE supports both *Time Division Duplexing* (TDD) and *Frequency Division Duplexing* (FDD). Both TDD and FDD are widely deployed and the decision about which duplexing format to adopt depends on the particular application. This Chapter is devoted to the FDD case.

OFDMA is used in downlink in order to obtain robustness against multipath interference and high affinity to advanced techniques such as frequency domain channel-dependent scheduling and *Multiple-Input Multiple-Output* (MIMO) antenna systems. Instead, *Single Carrier-Frequency Division Multiple Access* (SC-FDMA) is used in uplink in order to have a low *Peak-to-Average Power Ratio* (PAPR), user orthogonality in the frequency domain, and multi-antenna application. OFDMA divides the total stream into multiple sub-streams with lower data-rates. Each sub-stream is then mapped to an individual data sub-carrier that is modulated using QPSK, 16QAM, or 64QAM with different coding rate combinations. LTE uses bandwidths from 1.25, 2.5, 5.0, 10.0 to 20.0 MHz.

A *sub-channel* (i.e., a group of 12 sub-carriers) is the smallest logical allocation unit in the frequency domain; the *slot* (i.e., a group of 6–7 *symbols*) is the smallest allocation unit in the time domain. The LTE OFDMA frame structure can be considered like a grid, where a 10 ms radio frame is composed of ten 1 ms sub-frames (twenty 0.5 ms slots). The sub-frame time is also called *Transmission Time Interval* (TTI). The signal transmitted in each slot

is described by a resource grid of sub-carriers and available OFDM symbols. A *Physical Resource Block* (PRB) consists of one sub-channel for one slot of duration in time. Resource allocation to UEs is updated on a TTI basis. Then, PRBs are grouped into transport blocks that use the same *Modulation and Coding Scheme* (MCS). Table 1 describes the different modulation and coding combinations supported by LTE and indexed according to the *Channel Quality Indicator* (CQI) [4].

The *Signal-to-Interference and Noise* (SINR) thresholds for the AWGN case have been determined for the different MCSs with the corresponding efficiency η_i according to the following model and related formulas that have also been used to perform simulations in Ns-3 [5] and OMNeT++ [6]:

$$\eta_i = \log_2\left(1 + \frac{SINR_i}{\Gamma}\right) \quad \Rightarrow \quad SINR_i = 10\log_{10}\left[\Gamma\left(2^{\eta_i} - 1\right)\right] \text{ in dB} \qquad (1)$$

where $\Gamma = -\frac{2}{3}\ln\left(5 \times BER\right)$ and BER = 0.00005 and where the efficiency of the i-th MCS η_i can be determined on the basis of the data in Table 1 according to the following formula:

$$\eta_i = r_i \log_2\left(M_i\right) \quad \Rightarrow \quad 2^{\eta_i} = M_i^{r_i} \qquad (2)$$

For different channel conditions, $SINR_i$ conversions are adopted by introducing the concept of *Effective SINR* (ESINR). This is equivalent to take some margins on the SINR threshold values of the AWGN case.

LTE provides both *Hybrid ARQ* (H-ARQ) at PHY layer and ARQ at layer 2, supported by the RLC protocol. H-ARQ is a technique, combining *Forward Error Correction* (FEC) and *Automatic Repeat Request* (ARQ) methods, in which unsuccessful previous attempts are saved and used jointly with FEC retransmissions [7]. When the receiver fails to decode a transport block, it sends a *Negative-Acknowledgment* (NACK) to the transmitter, but it keeps bits from the failed attempt for future use. When the transmitter receives the NACK or a certain time elapses without any feedback, it retransmits new data to recover the missing transport block. LTE utilizes an *Incremental Redundancy* (IR) H-ARQ scheme with 1/3 turbo encoder (FEC code) and CRC for transport block error detection. IR entails to progressively send parity packets in each subsequent transmission. The receiver H-ARQ process performs a soft combination of the bits from the previous failed attempt with the currently-received retransmission. This permits to minimize the number of retransmissions. The maximum number of H-ARQ retransmissions is 3. The H-ARQ round trip time is 8 TTI. Each H-ARQ process is of the *Stop-And-Wait* (SAW) type. Multiple H-ARQ processes run in parallel to keep up the transmission of transport blocks, while the receiver is decoding already-received transport blocks. This method allows the continuous use of the transmission resources. As for the ARQ process operated at RLC layer, in the case of an error in a packet received at this layer, a packet retransmission is requested. The H-ARQ *Block Error Rate* (BLER) of a transport block is of the order of 10^{-1} after the first transmission, while the residual error rate of the packet delivered by H-ARQ to the RLC layer is of the order of 10^{-3} [8].

Table 1. Characteristics of the different transmission modes and SINR thresholds for AWGN channel conditions with *Single Input Single Output* (SISO) antenna scheme.

CQI_i	Modulations	Code rate r_i	Modulation size, M_i	SINR thresholds, $SINR_i$ (AWGN)
1	QPSK	78/1024	4	−2.1054
2	QPSK	120/1024	4	−0.1083
3	QPSK	193/1024	4	2.1776
4	QPSK	308/1024	4	4.5647
5	QPSK	449/1024	4	6.6514
6	QPSK	602/1024	4	8.4275
7	16QAM	378/1024	16	9.9379
8	16QAM	490/1024	16	11.8495
9	16QAM	616/1024	16	13.7624
10	64QAM	466/1024	64	14.9370
11	64QAM	567/1024	64	16.9703
12	64QAM	666/1024	64	18.8734
13	64QAM	772/1024	64	20.8506
14	64QAM	873/1024	64	22.6980
15	64QAM	948/1024	64	24.0546

1.2 Evolution Towards LTE-A

LTE systems have an increasing diffusion everywhere. The interest now is on gradually shifting towards a further LTE evolution, referred to as *LTE-Advanced* (LTE-A) [9]. This evolution will include significant improvements in terms of performance and capacity as compared to current LTE deployments.

The link performance of current cellular systems such as LTE is already quite close to the Shannon limit. From a pure link-budget perspective, the very high data-rates targeted by LTE-A require a higher SINR than that typically experienced in wide-area cellular networks. Although some link improvements are possible (e.g., using additional bandwidth or increasing the MCS efficiency), it is necessary to find approaches for improving the SINR level, such as allowing a denser infrastructure at reasonable costs. In particular, 3GPP LTE-A has proposed to use *Heterogeneous Network* (HetNet) deployments to improve system capacity and to provide a better coverage at hot spots [10]. The objective of HetNets is the improvement of the overall capacity as well as a cost-effective and green radio solution by deploying additional network nodes (i.e., eNBs) within the local area, such as low-power micro-/pico- network nodes, *Home-Evolved Node Bs* (HeNBs)/*Closed Subscriber Group* (CSG) cells, femto-cells, and relay nodes. Low-power micro-nodes and high-power macro-nodes can be maintained under the management of the same operator and share the same frequency bands. In this case, joint radio resource and interference management are

needed to avoid too high interference for low-power nodes. In some other cases, low- and high- power nodes can use discontinuous bands of an operator (carrier aggregation) so that mutual interference is avoided. Macro network nodes with large *Radio Frequency* (RF) coverage areas are deployed in a planned way for blanket coverage of urban, suburban, and rural areas. Instead, local nodes with small RF coverage areas aim to complement the macro network nodes for coverage extension or throughput enhancement. Moreover, global coverage can be provided by satellites (macrocells) according to an integrated system concept.

Another important innovation considered for LTE-A is the adoption of MIMO antenna solutions that are already used in LTE and will play an even more important role in LTE-A. Both Spatial Diversity MIMO and Spatial Multiplexing MIMO are supported by LTE-A. Moreover, 8×8 MIMO is adopted in downlink and 4×4 MIMO is envisaged for uplink transmissions. The selection of the type of MIMO depends on the channel quality: for situations with low SINR, it is better to use Spatial Diversity MIMO; instead, Spatial Multiplexing MIMO should be adopted in the presence of high SINR values.

2 Frequency Reuse Schemes

An important cell planning technique is to reuse the same frequency bands among sufficiently-separated cells so that the mutual interference among cells using the same frequency is negligible. There are several frequency reuse schemes that are characterized by different *Inter-Cell Interference* (ICI) levels, as detailed below.

2.1 Survey of Frequency Reuse Schemes

In a multi-cell network scenario employing frequency reuse across different cells, ICI occurs when neighbouring cells use the same frequency bands. The most severe form of ICI typically occurs on or near the edge of a cell. *ICI Coordination* (ICIC) techniques, whereby UEs in a cell are allocated with frequency resources that are orthogonal to all or to a part of the interfering UEs in adjacent cells, are needed to reduce ICI effects especially at cell borders. As such, various frequency reuse schemes have been proposed. The most straightforward approach is the so-called fixed frequency reuse scheme, whereby the whole bandwidth is divided into K non-overlapping parts that are assigned to K neighbouring cells. This frequency planning scheme allows to control ICI at the cost of a reduced spectral efficiency. A basic scheme is adopting a hexagonal cellular layout with $K = 3$.

A more refined frequency reuse scheme is *Fractional Frequency Reuse* (FFR), where different sets of sub-channels are allocated to the UEs in the cell-edge area of adjacent cells in order to control the ICI levels and where all spectrum can be used by UEs in the central part of the cell. All sub-channels are transmitted with the same power level. Different FFR variants are available, depending on the differentiation on the portions of bandwidth used in the cell centre and at cell edge. SFR is an enhancement of FFR in that there is a differentiation in the

transmission power for cell-centre UEs with respect to cell-edge UEs in order to reduce ICI at cell edge [11].

2.2 Soft Frequency Reuse

With SFR, UEs within each cell are divided into two groups (i.e., cell-centre UEs and cell-edge UEs), depending on the distance from the eNB. Cell-edge UEs are restricted to the reserved cell-edge bandwidth; instead, cell-centre UEs have exclusive access to the cell-centre bandwidth and can also have access to the cell-edge bandwidth, but with a lower priority than cell-edge UEs. Usually, the cell-edge bandwidth in one cell/sector is fixed to $1/K$-th of the whole bandwidth with the aim of ensuring that adjacent cells/sectors can allocate non-overlapping frequency bands to their cell-edge UEs [12,13]. K is called *Frequency Reuse Factor* (FRF). FRF of 1 is very attractive, but entails high ICI levels, thus impacting on the traffic capacity of a cell. FRF of 1 could be adopted only for those UEs closer to the eNB, let us say within a distance ρ_0. Instead, the external part of the cell should adopt a higher FRF level, denoted by K. This solution is implemented by the SFR scheme, as proposed by 3GPP LTE, where typically $K = 3$ [13]. Hence, $1/K$-th of the whole bandwidth BW is used in the external part of the cell, where packets are transmitted by the eNB with power level P_{Te} per sub-channel. Instead, the central part of the cell can even use the whole bandwidth BW, but with a lower transmission power P_{Tc} per sub-channel. Let us denote:

$$\rho_0 = \mu R_c \quad \text{and} \quad P_{Te} = \omega P_{Tc} \tag{3}$$

where $\mu \in (0, 1]$ denotes the normalized cell-centre radius (R_c is the maximum cell range for which we will use the same value as that of the classical frequency reuse K) and where $\omega > 1$ represents the border-to-centre power ratio. Of course P_{Te} and P_{Tc} depend on the transmission power available at the eNB (downlink case).

The reuse of resources with SFR and $K = 3$ is shown in Fig. 1, where the central part of the cell has a different colour to represent the fact that a full-frequency reuse can be adopted in that part of the cell. This figure also shows reference distances D_1, D_2, and R_c.

Considering a uniform UE distribution in the cell (circular cell with radius R_c) and adopting a *Round Robin* (RR) service discipline, the probability (or the percentage of time) that the eNB is transmitting to cell-centre UEs, β, is obtained as:

$$\beta = \frac{\pi \rho_0^2}{\pi R_c^2} = \left(\frac{\rho_0}{R_c}\right)^2 = \mu^2. \tag{4}$$

If a TTI is fully devoted to cell-centre UEs, the whole capacity BW is available to these UEs. Otherwise, if a TTI is used to allocate resources to both cell-centre UEs and cell-edge UEs, the capacity available to cell-centre UEs is $(K-1)BW/K$; instead, the capacity available for cell-edge UEs is BW/K. We refer here to this second case.

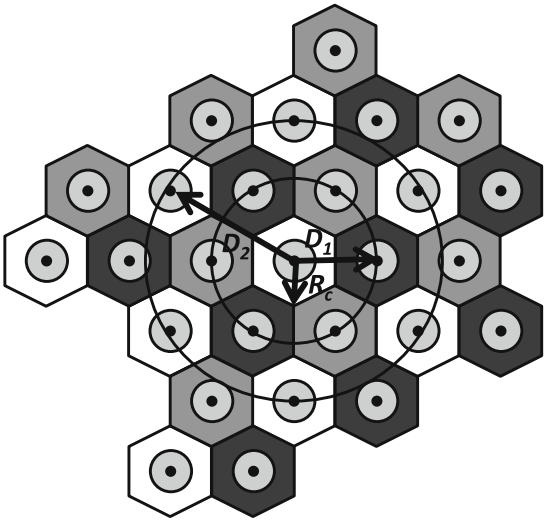

Fig. 1. System layout and frequency planning for the SFR scheme with $K = 3$.

Before concluding this Section, let us consider the implications of HetNets on cell planning with SFR; we can note that there might be strong interference for UEs in the areas where macro-cells are close to pico-cells. For instance, we can have a UE connected to a macro-cell and near a pico-cell. In this case, this UE will suffer from interference coming from the pico-cell [14]. To mitigate the interference, the macro-cell can assign a specific set of sub-channels to this UE, while we block this set of sub-channels in the pico-cell, by setting the power level in the pico-cell to 0 (or to a very small value) for this set of sub-channels. This technique is similar to what we have done so far with SFR, differentiating the sub-channels used in the cells as well as the power levels depending on the UE distance. This method entails some throughput reduction for pico-cells, but given the small numbers of UEs connected to them, this problem can be negligible. The main cell planning issue here is to define the criteria according to which there is the need to use pico-cells.

3 Capacity Evaluation with SFR and Optimization

Let S denote the total number of sub-channels in the whole bandwidth BW; S also corresponds to the number of PRBs per TTI divided by 2. Let T denote the number of sub-channels available at the edge of the cell. We consider the constraint that the total transmission power at the eNB on the whole bandwidth BW is equal to P_T. This entails the following condition to characterize P_{Tc} and P_{Te} expressing the fact that the sum of the transmission power on all sub-channels at the eNB is equal to P_T [13]:

$$P_T = \omega T P_{Tc} + (S - T) P_{Tc} \quad \Rightarrow \quad P_{Tc} = \frac{P_T}{\omega T + S - T} \tag{5}$$

Hence, according to the above formula (5) an increase in the cell-edge transmission power entails a reduction in the transmission power for cell-centre sub-channels. In the following SINR study for SFR, the noise level N is referred to the bandwidth of a sub-channel (i.e., BW/S) since the SINR itself is the ratio of powers received on a sub-channel: $N = kT_0BW/S$, where k is the Boltzmann constant and T_0 is the ambient temperature in Kelvin degrees.

The useful signal as well as interfering ones are characterized by power levels according to the following law, relating (sub-channel-based) transmission power P_{T_X} (corresponding to either P_{Tc} or P_{Te}, respectively for transmissions to cell-centre UEs or to cell-edge UEs) and the received power P_R:

$$P_R = \varphi \left(\frac{R}{R_c} \right)^{-\nu} P_{TX} \tag{6}$$

where φ and ν are determined according to the *Stanford University Interim* (SUI) model as follows [15]:

$$\varphi = \begin{cases} \left(\frac{R_0}{R_c}\right)^{\gamma} \left(\frac{\lambda}{4\pi R_0'}\right)^2 10^{\frac{-\left[s+X_f+X_h+L_T+L_R\right]+G_T+G_R}{10}}, & if\ \frac{R}{R_c} > \frac{R_0'}{R_c} \\ \left(\frac{\lambda}{4\pi R_c}\right)^2 10^{\frac{-[s+L_T+L_R]+G_T+G_R}{10}}, & if\ \frac{R}{R_c} \leq \frac{R_0'}{R_c} \end{cases}$$

$$\nu = \begin{cases} \gamma, & if\ \frac{R}{R_c} > \frac{R_0'}{R_c} \\ 2, & if\ \frac{R}{R_c} \leq \frac{R_0'}{R_c} \end{cases} \tag{7}$$

where $X_f = 6 \times \log_{10}(f\ [\text{GHz}]/2)$ is a correction factor for frequencies above 2 GHz (here, $f = 2.1$ GHz), $X_h = -d \times \log_{10}(h_{UE}/2)$ is a correction factor for the receiver antenna height (here, $h_{UE} = 1.5$ m is the UE antenna height), s represents a shadowing term (either a normal random variable in dB or a 95-th percentile term to take some planning margins), R_0 is a nominal reference distance of 100 m, and where the path loss exponent γ (depending on the propagation environment), α and R_0' (a threshold distance for a change in the path loss slope) are detailed in [3, 15].

Let φ^* denote the value of φ for $R > R_0$'. In this study, we use a fixed value for s (margin). The consideration of a normal distribution for s in dB (so that SINR becomes a random variable) is left to a future study. In the derivation of SINR, we consider the ratio of the transmission powers on groups of sub-carriers (a sub-channel); of course, we have to consider the same number of sub-carriers at numerator and denominator. As for R_c, we use the maximum cell range achievable by the classical reuse scheme with the same K value and the same link budget conditions (antenna, path loss, etc.) and referring to the most protected MCS level #1 with $SINR_1$, as shown in Table 1. This is an arbitrary choice, since also different R_c values could be considered. Basically, this choice allows to plan the cell range with no or small outage probability at cell border.

Please note that we could even consider other propagation models for the SFR study (e.g., the Hata model), but these aspects are beyond the scope of the present Chapter.

With SFR, we study the ICI level and then SINR by differentiating two cases: cell-centre UEs and cell-edge UEs. We limit the consideration of interfering signals to the first two tiers of adjacent cells with respect to a central reference cell (eNB). Moreover, as a first approximation, we denote by D_1 and D_2 the distances of a reference UE from the interfering eNBs of the first and second tier of adjacent cells, respectively. These distances are approximated as the distances between the eNB of our reference UE and the eNBs of the interfering cells: $D_1 = \sqrt{3}R_c$ and $D_2 = \sqrt{3K}R_c$.

For cell-centre UEs (referring to the white reference cell at the centre of Fig. 1), there are interfering transmissions in both the first and the second tiers of adjacent cells. As for the first tier, the interference power with level I_{c1} is the result of 3 interfering transmissions to cell-centre UEs with transmission power P_{T_c} per sub-channel (gray and darkest adjacent cells) and 3 interfering transmissions to cell-edge UEs with transmission power P_{T_e} per sub-channel (gray and darkest adjacent cells).

$$I_{c1} = 3\varphi^* \left(\frac{D_1}{R_c}\right)^{-\gamma} P_{Tc} + 3\varphi^* \left(\frac{D_1}{R_c}\right)^{-\gamma} P_{Te} \tag{8}$$

As for the second tier, the interference power with level I_{c2} is the result of 9 interfering transmissions to cell-centre UEs with transmission power P_{T_c} per sub-channel (white, gray, and darkest cells) and 3 interfering transmissions to cell-edge UEs with transmission power P_{T_e} per sub-channel (gray and darkest cells).

$$I_{c2} = 9\varphi^* \left(\frac{D_2}{R_c}\right)^{-\gamma} P_{Tc} + 3\varphi^* \left(\frac{D_2}{R_c}\right)^{-\gamma} P_{Te} \tag{9}$$

In conclusion, we have:

$$I_c = I_{c1} + I_{c2} \tag{10}$$

For cell-edge UEs, we adopt the same approach to determine the interference coming from the first and the second tiers of adjacent cells. As for the first tier, the interference power with level I_{e1} is the result of 3 interfering transmissions to cell-centre UEs with transmission power P_{Tc} per sub-channel (gray adjacent cells) and 3 interfering transmissions to cell-centre UEs with transmission power P_{T_c} per sub-channel (the darkest adjacent cells).

$$I_{e1} = 6\varphi^* \left(\frac{D_1}{R_c}\right)^{-\gamma} P_{Tc} \tag{11}$$

As for the second tier, the interference power with level I_{e_2} is the result of 6 interfering transmissions to cell-edge UEs with transmission power P_{T_e} per sub-channel (white cells) and 6 interfering transmissions to cell-centre UEs with

transmission power P_{Tc} per sub-channel (gray and darkest cells).

$$I_{e2} = 6\varphi^* \left(\frac{D_2}{R_c}\right)^{-\gamma} P_{Te} + 6\varphi^* \left(\frac{D_2}{R_c}\right)^{-\gamma} P_{Tc} \tag{12}$$

In conclusion, we have:

$$I_e = I_{e1} + I_{e2} \tag{13}$$

We consider that interfering signals always travel a distance greater than R_0' so that they are characterized by $\varphi = \varphi^*$ and $\nu = \gamma$. In order to derive the SINR for cell-centre UEs, $SINR_c$, we consider that our reference UE is at a distance $R \leq \rho_0$ from its eNB, that $P_{T_X} \equiv P_{Tc}$ and that the power received is according to (6). Instead, in order to express the SINR for cell-edge UEs, $SINR_e$, we consider that our reference UE is at a distance $R > \rho_0$ from its eNB and $P_{T_X} \equiv P_{Te}$. Then, SINR as a function of the distance R of the UE from its eNB is determined by $SINR_c$ in (14) for $R \leq \rho_0$ and by $SINR_e$ in (15) for $R > \rho_0$ according to the formulas below where ν and φ also depend on R/R_c:

$$SINR_c\left(\frac{R}{R_c}, \mu, \omega, P_{Tc}\right) = \frac{\left(\frac{R}{R_c}\right)^{-\nu}}{\frac{3\varphi^*}{\varphi}\left[(1+\omega)\left(\sqrt{3}\right)^{-\gamma} + (3+\omega)\left(\sqrt{3K}\right)^{-\gamma}\right] + \frac{N}{\varphi P_{Tc}}} \tag{14}$$

$$SINR_e\left(\frac{R}{R_c}, \mu, \omega, P_{Tc}\right) = \frac{\left(\frac{R}{R_c}\right)^{-\nu}}{\frac{6\varphi^*}{\varphi}\left[\frac{1}{\omega}\left(\sqrt{3}\right)^{-\gamma} + \left(1+\frac{1}{\omega}\right)\left(\sqrt{3K}\right)^{-\gamma}\right] + \frac{N}{\varphi\omega P_{Tc}}} \tag{15}$$

SINR behaviours for different μ and ω values are shown in Fig. 2 for $P_T = 37\,\text{dBm}$, $BW = 5\,\text{MHz}$ and 'intermediate' propagation conditions [15]. From this graph, we can see that the SINR curve has a discontinuity at $R = \rho_0$ due to the change in the conditions for interference, transmission power, and available bandwidth.

This approach to determine SINR could be easily adapted to model cell sectorisation. In this case, we should reduce the number of interfering cells and add the antenna gain to the link budget. Further details on cell sectorisation are beyond the scope of the present work. However, we believe that the following SFR optimization approach is also valid for a sectorised scenario.

The aim of the following study is to present traffic engineering implications for planning the LTE coverage with SFR so that the rough approximation of circularly-shaped cells (radius R_c) is acceptable. We assume that the UEs serviced by an eNB are uniformly distributed in the cell. Hence, the number of UEs receiving transmissions according to a certain MCS (or the corresponding CQI) is proportional to the area within the cell that is covered by that MCS mode.

If SINR does not monotonically decrease with the distance, as in our SFR case, the same CQI_i value can be adopted in two disjoint rings: one for distances lower than ρ_0 and another for distances greater than ρ_0. Let A_{ci} denote the area of the ring in the cell-centre zone where mode CQI_i is used. Moreover, let A_{ei} denote the area of the ring in the cell-edge zone where mode CQI_i is used. Areas A_{ci} and A_{ei} are disjoint. The total area where the transmission mode

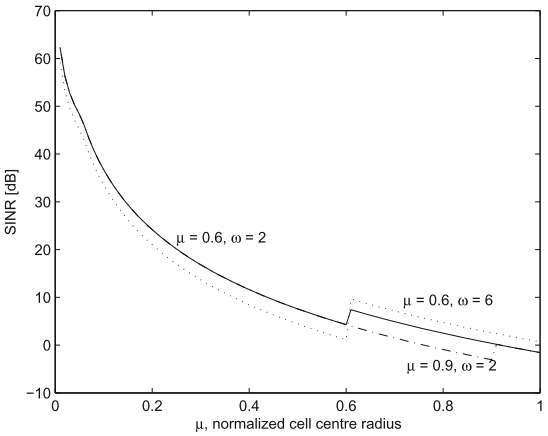

Fig. 2. Examples of SINR behaviour.

corresponding to CQI_i is used is $A_i = A_{ci} + A_{ei}$. This area can be formally characterized by the radii fulfilling the following condition:

$$SINR_i \leq SINR\left(\frac{R}{R_c}, \mu, \omega, P_{Tc}\right) < SINR_{i+1}. \tag{16}$$

Area A_{ci} is limited by radii $R_{c,i}$ and $R_{c,i_{+1}}$ so that $0 \leq R_{c,i_{+1}} \leq R_{c,i} \leq \rho_0$. Moreover, A_{ei} is limited by radii $R_{e,i}$ and $R_{e,i_{+1}}$ so that $\rho_0 \leq R_{e,i_{+1}} \leq R_{e,i} \leq R_c$. In these conditions, $R_{c,i}$ is obtained by solving $SINR_c = SINR_i$ using the $SINR_c$ expression in (14). In case of no solution in the range $0 - \rho_0$ for this SINR condition, we take the limiting value 0 or ρ_0 for $R_{c,i}$, depending on the fact that the threshold value $SINR_i$ is too high or too low for the $SINR_c$ values for cell-centre UEs. If $SINR_1$ is too high, we have outage in the cell centre. Moreover, $R_{e,i}$ is obtained by solving $SINR_e = SINR_i$ using the $SINR_e$ expression in (15). In case of no solution in the range $\rho_0 - R_c$ for this SINR condition, we take the limiting value ρ_0 or R_c for $R_{e,i}$, depending on the fact that the threshold value $SINR_i$ is too high or too low for the $SINR_e$ values for cell-edge UEs. If $SINR_1$ is too high, we have outage at the cell border.

Let Ω_{ci} denote the probability that mode CQI_i is used for cell-centre UEs and Ω_{ei} the probability that mode CQI_i is used for cell-edge UEs. These probabilities are obtained as:

$$\Omega_{ci} = \frac{A_{ci}}{\pi R_c^2} \quad \text{and} \quad \Omega_{ei} = \frac{A_{ei}}{\pi R_c^2} \quad \text{for } i = 1, \ldots, 15 \tag{17}$$

Note that probabilities Ω_{ci} and Ω_{ei} above are normalized on the whole cell area and not on the area of the part (cell-centre or cell-edge) they refer to. We consider Ω_{ci} for $i = 0$ to represent the outage probability in the cell-centre area (i.e., outage occurs in the cell-centre area if the condition $SINR_c < SINR_1$ is fulfilled) and we consider Ω_{ei} for $i = 0$ to represent the outage probability

in the cell-edge area (i.e., outage occurs in the cell-edge area if the condition $SINR_e < SINR_1$ is fulfilled). The following condition is met:

$$\sum_{i=1}^{15} (\Omega_{ci} + \Omega_{ei}) \leq 1 \tag{18}$$

where equality is valid only when there is no outage. The overall outage probability is given by $\Omega_{c_0} + \Omega_{e_0}$.

Probabilities Ω_{ci} and Ω_{ei} for $i = 1, \ldots, 15$ can be derived as shown below:

$$\begin{aligned} \Omega_{ci}\left(SINR_i, SINR_{i+1}, \mu, \omega, K, P_{T_c}\right) &= \frac{\pi R_{c,i}^2 - \pi R_{c,i+1}^2}{\pi R_c^2} = \left(\frac{R_{c,i}}{R_c}\right)^2 - \left(\frac{R_{c,i+1}}{R_c}\right)^2 \\ \Omega_{ei}\left(SINR_i, SINR_{i+1}, \mu, \omega, K, P_{T_c}\right) &= \frac{\pi R_{e,i}^2 - \pi R_{e,i+1}^2}{\pi R_c^2} = \left(\frac{R_{e,i}}{R_c}\right)^2 - \left(\frac{R_{e,i+1}}{R_c}\right)^2 \end{aligned} \tag{19}$$

The dependence of probabilities Ω_{ci} and Ω_{ei} on P_{Tc} (or equivalently P_T) is negligible. These probabilities are used below to express the mean PHY-layer capacity of a cell.

The cell capacity with a certain CQI_i is obtained under the scheduling assumption that all PRBs of a TTI are transmitted with the same modulation and coding scheme of that CQI_i and this is possible because we consider that the system is fully loaded both in its central area and in its edge area. We consider the gross cell capacity, including the capacity spent for control channels. Moreover, we differentiate between cell-centre capacity C_{ci} and cell-edge capacity C_{ei}, since the available bandwidth BW is divided between cell-centre and cell-edge parts according to the coefficients $(K-1)/K$ and $1/K$. We have:

$$\begin{aligned} C_{ci} &= 12 \times 7 \times \eta_i \times \frac{(K-1) \times N_{PRB}(BW)}{K \times TTI} \\ C_{ei} &= 12 \times 7 \times \eta_i \times \frac{N_{PRB}(BW)}{K \times TTI} \end{aligned} \tag{20}$$

where $TTI = 1\,\text{ms}$ and $N_{PRB}(BW)$ is the number of PRBs per TTI, considering the whole available bandwidth, BW [3].

We obtain the average PHY-layer capacity of a cell, C, by summing the capacities C_{ci} and C_{ei} weighted by the probabilities of using CQI_i in the cell centre or in the cell edge:

$$\begin{aligned} C\left(\mu, \omega, BW, K, P_{Tc}\right) &= \textstyle\sum_{i=1}^{15} \left\{C_{ci} \times \Omega_{ci} + C_{ei} \times \Omega_{ei}\right\} = \\ &= \textstyle\sum_{i=1}^{15} \left\{\eta_i \left[(K-1)\ \Omega_{ci} + \Omega_{ei}\right]\right\} \frac{12 \times 7 \times N_{PRB}(BW)}{K \times TTI} \end{aligned} \tag{21}$$

Note that the dependence on thresholds $SINR_i$ has been omitted in the notation of the mean cell capacity C. We can use (21) to select the values of μ and ω that maximize the cell capacity. Figure 3 shows the behaviour of the capacity C as a function of μ and ω for $P_T = 37\,\text{dBm}$, $BW = 5\,\text{MHz}$, 'intermediate' propagation conditions, and AWGN channel, according to the SINR thresholds in Table 1. Note that if there is outage in the cell for a given configuration of μ and ω, we have considered in the following graphs a cell capacity equal to

zero (even if the actual cell capacity is not zero) in order to make it evident that some configurations of μ and ω correspond to outage conditions. Hence, in Fig. 3 the darkest area corresponds to outage configurations in the cell of radius R_c; these configurations are not good for cell planning purposes. The graph in Fig. 3 shows that the PHY-layer cell capacity C has an optimal configuration (maximum) for μ around 0.8 and ω around 1.6. The results in Fig. 3 are quite insensitive to variations of P_T (only the cell range changes).

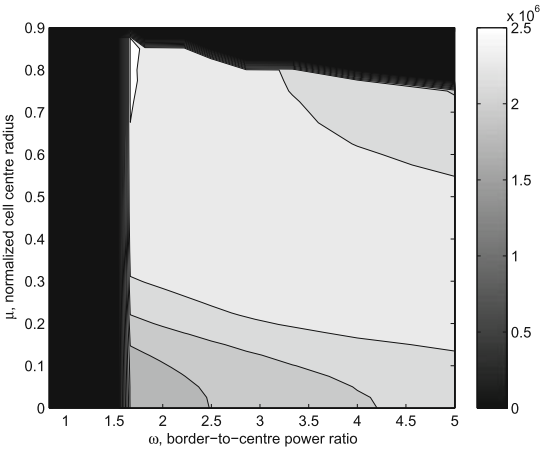

Fig. 3. PHY-layer capacity as a function of μ and ω in the AWGN channel case. The side bar maps the gray scale to the capacity in bit/s.

Similar results to those in Fig. 3 could be achieved considering MAC-layer capacity including the effects of H-ARQ retransmissions.

4 Simulation Results

In this Section, we present simulation results to analyse the capacity of LTE with SFR. The following system configuration has been adopted for all simulations:

- SUI propagation model for an intermediate scenario
- System bandwidth $BW = 5\,\text{MHz}$
- Omni-directional antennas at both eNBs and UEs
- eNB transmission power $P_T = 37\,\text{dBm}$
- Uniform UE distribution in the cells
- Cell range R_c equal to 1666 m (AWGN channel), the reference value of the classical frequency reuse with $K = 3$
- Cellular hexagonal layout with a reference central cell (eNB) and 18 adjacent cells (1st and 2nd tiers of cells)
- Shadowing margin $s = 15.8\,\text{dB}$

– SFR with cell-edge reuse factor $K = 3$
– In order to simplify the model, we have assumed that all sub-carriers (sub-channels) experience the same SINR conditions.
– SINR thresholds are used for the different CQIs according to Table 1.

4.1 Model Validation with the Ns-3 Simulator of LTE

The Ns-3 environment already supports an LTE simulator [5]. In order to get the SFR scheme included in Ns-3, we have modified the resource allocator module. In particular, SFR for $K = 3$ is implemented as follow: assuming that the system is fully loaded, cell-edge UEs are allowed to use only 1/3 of the whole bandwidth BW, instead cell-centre UEs are scheduled to use the rest 2/3 of the bandwidth. The channels used by cell-edge UEs are set to be different from those of the six adjacent cells in order to mitigate interference. The transmission power for one sub-channel for cell-edge UEs is ω times higher than that for cell-centre UEs. In order to study the cell capacity when the system is fully loaded (downlink traffic), we consider that the eNB transmits to each UE in the cell a UDP traffic at the maximum possible bit-rate for the bandwidth considered; this is done in order to consider the interference levels in the most critical conditions. Each eNB uses pilot channels (i.e., PDCCH + PCFIC) to send reference signals to UEs that, in turn, calculate SINR of each PRB by dividing the power of the signal from the eNB by the sum of the noise power plus all powers received on the same PRB and coming from interfering eNBs. The calculation of SINR is used to determine the CQI level sent to eNB by a feedback signal. The MCS of each sub-channel corresponds to the CQI level of that sub-channel. In our study, all sub-channels used by a UE have the same CQI value. Referring to the simulation area of 19 cells, we consider UEs randomly placed in the cells and we categorize them as in the cell-centre area or in the cell-edge one depending on the distance from their eNB. Then, we measure the SINR for each UE in the central cell and determine the corresponding cell capacity as the average of the capacity provided to the UEs in the different parts of this cell.

The graph in Fig. 4 shows the comparison between the SINR behaviour from the analysis in Sect. 3 and that obtained from Ns-3 simulations in the AWGN channel case. We can note that the agreement is quite good and that there is a slight difference when approaching cell borders due to the approximations in the analysis on the derivation of the distance of interferers.

The following graph in Fig. 5 shows the capacity (net capacity without control channels) obtained from Ns-3 simulations for different combinations of ω and μ, assuming an RR scheduler that is consistent with the assumptions made in Sect. 2. These results have been obtained considering fixed users and outage conditions. These results show that the optimal configuration is quite close to that predicted by the theoretical approach in Sect. 3; some small differences are due to following issues: (*i*) the rough granularity (steps of 0.1 for both μ and ω) adopted for performing simulations; (*ii*) the inclusion of the control channels capacity in the total capacity in the analysis (control channels roughly entail a 14 % capacity overhead).

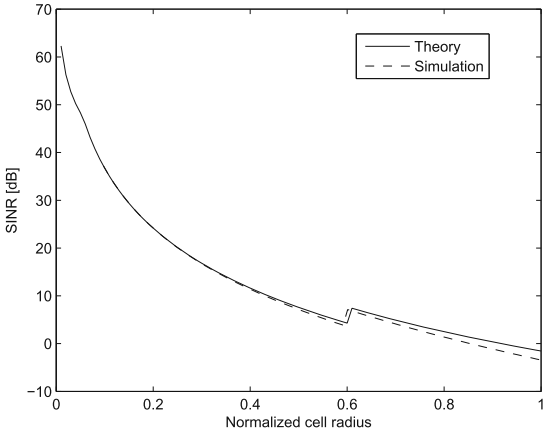

Fig. 4. SINR behaviours from Ns-3 simulations and the theory in the AWGN channel case for $\omega = 2$ and $\mu = 0.6$.

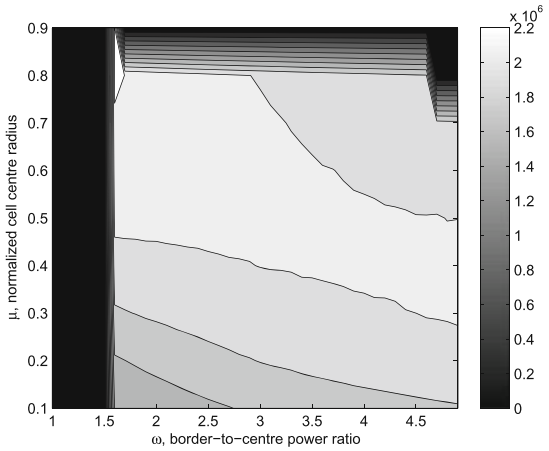

Fig. 5. Capacity with SFR from simulations for AWGN channel and different values of the normalized cell-centre radius μ and border-to-centre power ratio ω.

4.2 Impact of Mobility on SFR Cell Capacity

Client (UE) mobility heavily influences the performance of wireless networks. In the analysis carried out in the previous part of this Chapter, we have assumed that clients are uniformly distributed in the cell and that clients' locations do not change. This is not the case of the real world, where clients move while they exchange traffic through the LTE network. The distribution of client positions within the area covered by the cell influences its capacity, because clients close to the eNB can communicate using more effective MCS levels. In this Section, we evaluate the impact of mobility on cell capacity with SFR via simulations.

An OMNeT++ [6] simulation model has been implemented that supports all the characteristics highlighted at the beginning of Sect. 4.

The OMNeT++ simulation area consists of 19 eNBs located as shown in Fig. 1. Only the capacity of the central cell was analyzed. It is assumed that all clients request best effort traffic and that the RR scheduler is adopted. We consider the whole capacity of a cell, also including control channels capacity. The cell capacity is calculated as the average of the throughput offered to all UEs within range. The throughput of a UE was calculated using the SUI propagation model (as in Sect. 3), assuming a total transmission power $P_T = 37\,\text{dBm}$ and $BW = 5\,\text{MHz}$. The calculation of cell capacity was repeated every 100 ms of the simulation time to evaluate how it changes in response to the changing locations of network nodes (it corresponds on average to 0.5 m change in client location). The simulation time has been set to 10 days and we have obtained both average and standard deviation of cell capacity. The number of clients of the cell was set to 100. These clients were roaming within the area covered by the eNB according to a mobility model as detailed below.

Four different client mobility models have been implemented: *Random Waypoint* (RW) [16], *Gauss-Markov* (GM) [17], *Mass Mobility* (MM) [18], and *Real Life Mobility Model* (RLMM) [19]. The mean speed of a client has been set to 18 km/h in all mobility models. At the start of the simulation, all clients are uniformly spatially distributed: they are on a grid with equal distances of 100 m from each other. The comparison of the capacity results obtained with the different mobility models is shown in Fig. 6 for a configuration with $\mu = 0.8$ and $\omega = 1.6$, as selected in Sect. 3.

In the RW mobility model, nodes are moving directly to the next randomly-chosen point (waypoint). The move between two points is according to a straight line with constant speed. When a node reaches the next point, it waits for some time and then chooses a new destination. In the MM model, nodes have a certain mass and apply a momentum accordingly. Nodes move in a straight line for a certain time interval (5 s on average) and make a turn with an angle randomized around the previous angle, using a normal distribution with an average of 30 degrees. Node speed is normally distributed. When a node reaches the boundary of the simulated area, it reflects off the wall according to the same angle. The lower rate of changes in the movement makes cell capacity changes much smaller on a short time scale, but the correlation of the movement may cause quite high changes in the total cell throughput. RLMM simulates the changes of human behaviour in relation to weekly and daily cycles. The day is divided into periods during which human movement patterns are very different, like for instance the 8 h working time or the 8 h sleeping time (when the client does not move) and the travel time from the work place to home (when the client intensively moves between two points on the simulated area). The simulations have shown that these patterns very heavily influence the mean cell capacity: it is almost constant during nighttimes (when clients do not change the location and have constant modulation) and rapidly changes during the periods of heavy commuting to and from work. The GM mobility model assumes that mobile nodes have an initial

speed and direction, and takes this into consideration to compute the values for the next step. Thus, the movement is much more smoothed, but the traveled distances are higher than in other models, so that capacity has a higher variation.

Comparing the results of the different mobility patterns we can notice that the average cell capacity is similar for GM and MM models, but the RW model gives much higher average cell capacity. In any case, all mobility models yield higher cell capacity values than those considered in Sect. 3, because all mobility models tend to distribute the clients close to the cell centre; this phenomenon is emphasized in the case of the RW mobility model [20]. The standard deviation of the cell capacity changes significantly from model to model. From the RLMM model we can see that the changes in human movement characteristics during day and night make the variance of cell capacity much higher than one could anticipate from simpler mobility models, because there are long periods with constant capacity (nigh time and working time), as can be seen in Fig. 8 in the next Sub-section.

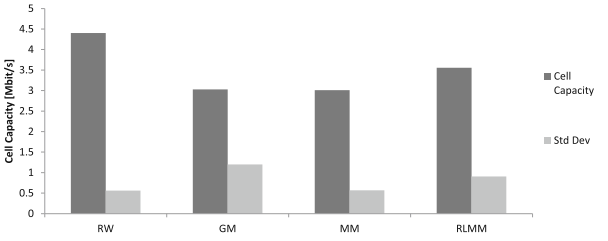

Fig. 6. Average and standard deviation of cell capacity for RW, GM, MM, and RLMM mobility models for normalized cell-centre radius $\mu = 0.8$ and border-to-centre power ratio $\omega = 1.6$.

4.3 Simulation Study of SFR Under Different Scheduling Policies

In the previous analysis, we have assumed that the transmission time (amount of PRBs) is allocated evenly among all mobile clients, as in the case of the RR scheduling algorithm. However, in addition to the RR scheduler, we consider the *Proportional Fair* (PF) scheduler [21]. With RR, every client UE is scheduled for equal times allocated without taking the channel quality into account. This entails the allocation of the same amount of PRBs to every client, assuming that there are always data available for transmissions. Depending on the MCS level used by each client, the transmission rate may be very different from client to client. With PF, each data flow is assigned with a data rate or a scheduling priority (depending on the implementation) that is inversely proportional to its anticipated resource consumption. PF ensures that every client can transmit the same amount of data, regardless of the channel quality. The goal is to guarantee fairness among flows. PF is a scheduling option well suited to non-real time traffic.

To evaluate how cell capacity is influenced by the scheduler, we have implemented both RR and PF schedulers within the OMNeT++ model [22] in the

SFR scenario. The simulations have been executed according to the parameters shown at the beginning of Sect. 4. In the following Figs. 7 and 8, the cell capacity has been compared between the two scheduling algorithms, considering the four mobility models under investigation. We can note that the PF scheduler heavily decreases the total cell capacity. This is caused by more PRBs allocated to serve clients with lower MCS levels to maintain the fairness of throughput provided by the eNB to its clients. The PF scheduler also decreases the amplitude of capacity changes. This can be seen in particular for the RLLM mobility model, since the cell capacity with PF is much steadier than that with the RR scheduler.

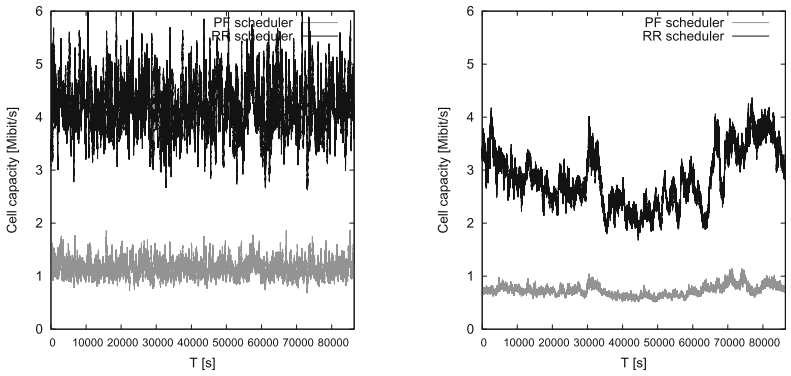

Fig. 7. Cell capacity in time for RW (left) and MM (right) mobility models with RR scheduler (black) or PF scheduler (grey) for SFR with normalized cell-centre radius $\mu = 0.8$ and border-to-centre power ratio $\omega = 1.6$ for 24 h of simulation time.

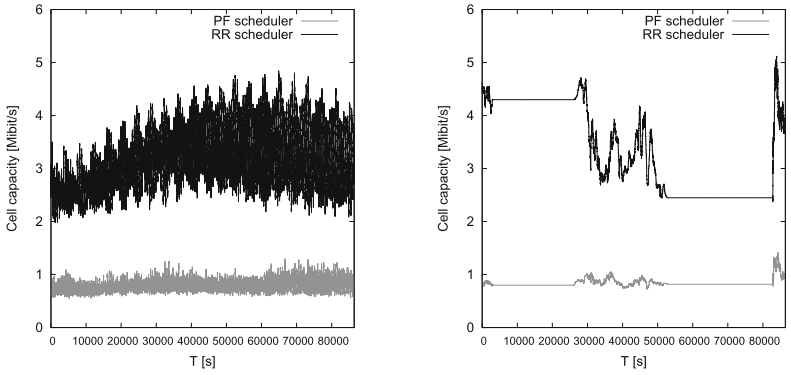

Fig. 8. Cell capacity in time for GM (left) and RLMM (right) mobility models with RR scheduler (black) or PF scheduler (grey) for SFR with normalized cell-centre radius $\mu = 0.8$ and border-to-centre power ratio $\omega = 1.6$ for 24 h of simulation time.

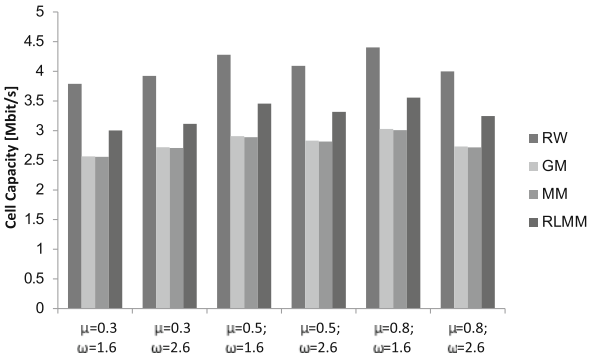

Fig. 9. Average cell capacity for RR scheduler with different mobility models and different SFR parameters.

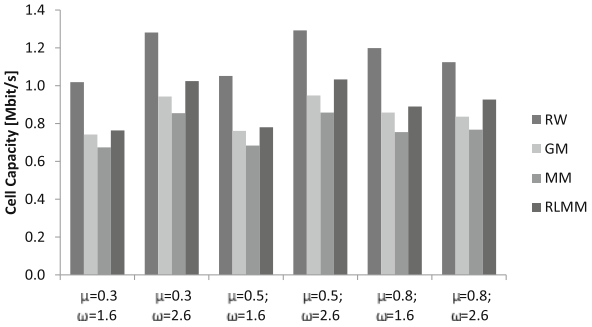

Fig. 10. Average cell capacity for PF scheduler with different mobility models and different SFR parameters.

The mobility models may distribute the users in the cell in different ways (especially in terms of the closeness to the eNB) [20], what creates different average capacity values and different optimization conditions for μ and ω with respect to those considered in Sect. 3. Thus, we have carried out simulations to evaluate the cell capacity in configurations where μ and ω are around the optimized point, as identified in the previous Section: $\mu = 0.8$ and $\omega = 1.6$. In particular, we have considered 6 points distributed in the μ - ω plane near the optimal point: that is μ between 0.3 and 0.8 and ω between 1.6 and 2.6. Results are shown in Figs. 9 and 10 for RR and PF schedulers, respectively. We can note that the results in Fig. 9 show that the optimum point is for $\mu = 0.8$ and $\omega = 1.6$, and this is consistent with the results of the analysis in Sect. 3 (Fig. 3) and those of the Ns-3 simulations in Subsect. 4.1 (Fig. 5). Instead, the results in Fig. 10 provide a different optimum point, because the PF scheduler is adopted; nevertheless, the configuration with $\mu = 0.8$ and $\omega = 1.6$ still provides a high capacity close to the maximum in this case. In Figs. 9 and 10, there are quite large differences in cell capacity between RW and the other mobility

models, because the RW mobility model tends to concentrate (more than the other mobility models) the users close to the cell centre. As already explained, this effect that is present in all mobility models [20,23] justifies the difference in capacity between the analysis in Sect. 3 and the simulation results shown in Subsects. 4.2 and 4.3.

5 Conclusions

In this Chapter, we have presented a framework to analyse the capacity of multi-cellular LTE systems based on soft frequency reuse. A system model has been proposed in order to characterize the SINR depending on two SFR important parameters, such as the normalized cell-centre radius μ and the border-to-centre power ratio ω. An optimization of these parameters has been carried out by means of analysis, Ns-3 simulations, and OMNeT++ simulations. We have also shown that the cell capacity and the SFR optimization are also influenced by the scheduling technique used at the eNB in order to manage the different traffic flows as well as by the different mobility patterns of the users. We have shown that the configuration with $\mu = 0.8$ and $\omega = 1.6$ provides maximum (or close-to-maximum) cell capacity values in many mobility and scheduling conditions.

A possible future work will deal with the study of SFR for the HetNet scenario, with modelling SFR in the MIMO case, and with the study of the effects of the lognormally-distributed shadowing.

Acknowledgments. This work has been in part supported by a grant of Polish National Center for Research and Development no. LIDER/10/194/L-3/11.

References

1. Cisco White Paper: Cisco Visual Networking Index: Global Mobile Data Traffic Forecast Update, 2013–2018, 5 February 2014
2. Ali-Yahiya, T.: LTE and Its Performance. Springer, New York (2011)
3. Giambene, G., Ali-Yahiya, T.: LTE planning for soft frequency reuse. In: Proceedings of Wireless Days 2013, Valencia, Spain, 13–15 November 2013
4. 3GPP: E-UTRA Multiplexing and Channel Coding, TS 36.212, Release 12 (2013)
5. LTE simulator for Ns-3. http://lena.cttc.es/manual/lte-design.html#H-ARQ
6. Varga, A., Hornig, R.: An overview of the OMNeT++ simulation environment. In: Proceedings of the 1st International Conference on Simulation Tools and Techniques for Communications, Networks and Systems and Workshops (Simutools'08), Belgium (2008)
7. 3GPP: Medium Access Control (MAC) Protocol Specification, TS 36.321 V12.0.0 (2013-12)
8. Park, H.-S., Lee, J.-Y., Kim, B.-C.: TCP performance degradation of in-sequence delivery in LTE link layer. Int. J. Adv. Sci. Technol. **37**, 27–36 (2011)
9. Ghosh, A., Ratasuk, R., Mondal, B., Mangalvedhe, N., Thomas, T.: LTE-advanced: next-generation wireless broadband technology. IEEE Wireless Commun. **17**(3), 10–22 (2010)

10. Hu, R.Q., Qian, Y., Kota, S., Giambene, G.: HetNets - a new paradigm for increasing cellular capacity and coverage [Guest Editorial]. IEEE Wireless Commun. **18**(3), 8–9 (2011). (Special issue)
11. Yu, Y.: Network planning for transparent mode IEEE 802.16j relay-based network. Ph.D. thesis, University College Dublin, Ireland (2010)
12. Novlan, T.D., Ganti, R.K., Ghosh, A., Andrews, J.G.: Analytical evaluation of fractional frequency reuse for OFDMA cellular networks. IEEE Trans. Wireless Commun. **10**(12), 4294–4305 (2011)
13. Xie, Z., Walke, B.: Enhanced fractional frequency reuse to increase capacity of OFDMA systems. In: Proceedings of the 3rd International Conference on New Technologies, Mobility and Security (NTMS 2009), Cairo, Egypt (2009)
14. Kosta, C., Hunt, B., Quddus, A.U., Tafazolli, R.: On interference avoidance through inter-cell interference coordination (ICIC) based on OFDMA mobile systems. IEEE Commun. Surv. Tutorials **15**(3), 973–994 (2013)
15. Erceg, V., Greenstein, L.J., Tjandra, S.Y., Parkoff, S.R., Gupta, A., Kulic, B., Julius, A.A., Bianchi, R.: An empirically-based path loss model for wireless channels in suburban environments. IEEE J. Sel. Areas Commun. **17**(7), 1205–1211 (1999)
16. Hyytia, E., Virtamo, J.: Random waypoint mobility model in cellular networks. Wireless Netw. **13**, 177–188 (2007)
17. Ariyakhajorn, J., et al.: A comparative study of random waypoint and Gauss Markov mobility models in performance evaluation of MANET. In: Proceedings of the International Symposium on Communication and Information Technologies, ISCIT-06 (2006)
18. Perkins, C.E., Wang, K.: Optimized smooth handoffs in mobile IP. In: Proceedings of the Fourth IEEE Symposium on Computers and Communications (ISCC '99) (1999)
19. Gorawski, M., Grochla, K.: The real-life mobility model: RLMM. In: Proceedings of the Second International Conference on Future Generation Communication Technologies, London (2013)
20. Bettstetter, C., Wagner, C.: The spatial node distribution of the random waypoint mobility model. In: Proceedings of the WMAN Conference, Ulm, pp. 41–58 (2002)
21. Kwan, R., Leung, C., Zhang, J.: Proportional fair multiuser scheduling in LTE. IEEE Sign. Process. Lett. **16**(6), 461–464 (2009)
22. Varga, A.: The OMNeT++ discrete event simulation system. In: Proceedings of the European Simulation Multiconference (ESM2001), Prague, Czech Republic (2001)
23. Mousavi, M.S., et al.: Mobisim: a framework for simulation of mobility models in mobile ad-hoc networks. In: Proceedings of the Wireless and Mobile Computing, Networking and Communications Conference 2007 (WiMOB 2007) (2007)